FACTA UNIVERSITATIS
Series: **Mechanical Engineering**
https://doi.org/10.22190/FUME201221005P

Original scientific paper

SHAPE OF A SLIDING CAPILLARY CONTACT DUE TO THE HYSTERESIS OF CONTACT ANGLE: THEORY AND EXPERIMENT

Valentin L. Popov[1,2], Iakov A. Lyashenko[1,3], Jasminka Starcevic[1,2]

[1]Technische Universität Berlin, Germany
[2]National Research Tomsk State University, Russia
[3]Sumy State University, Ukraine

Abstract. *We consider a classical problem of a capillary neck between a parabolic body and a plane with a small amount of liquid in between. In the state of thermodynamic equilibrium, the contact area between the bodies and the liquid layer has a circular shape. However, if the bodies are forced to slowly move in the tangential direction, the shape will change due to the hysteresis of the contact angle. We discuss the form of the contact area under two limiting assumptions about the friction law in the boundary line. We also present a detailed experimental study of the shape of sliding capillary contact in dependence on the roughness of the contacting surfaces.*

Key words: *Capillarity, Contact Angle Hysteresis, Friction, Contact Area, Roughness*

1. INTRODUCTION

Since Coulomb, it is known that the force of dry friction may depend on humidity of the atmosphere [1, 2]. As a physical reason for this dependency, formation of capillary bridges is considered [3], because in a complete cycle of formation and destruction of a capillary bridge a certain amount of energy is dissipated. However, even if the capillary bridges are not destroyed, they can contribute to friction due to the dry friction experienced by the boundary line of a capillary bridge. The friction in the boundary line leads to the well-known effect of contact angle hysteresis [4]. As the contact angle determines the height of a capillary bridge, the contact angle hysteresis will lead to some deformation of the contact area.

Received December 21, 2020 / Accepted January 20, 2021
Corresponding author: Valentin L. Popov
Affiliation: Technische Universität Berlin, Sekr. C8-4, Straße des 17. Juni 135, D-10623 Berlin
E-mail: v.popov@tu-berlin.de

Contact angle hysteresis is studied intensively both theoretically [5, 6] and experimentally [7-10]. Heterogeneity of the surface is considered as the main physical reason for contact hysteresis. In [5], a liquid drop was considered on a porous surface, the pores of which were filled with another liquid. This situation is observed in lubricated systems in the presence of heterogeneous liquid inclusions in the lubricating layer. In [7], the effect of roughness on the hysteresis of the contact angle and on the work performed when a drop spreads over a rough surface is studied. It was found that these quantities nonlinearly depend on the roughness amplitude. It should be noted that RMS roughness was used for characterizing the roughness, which does not determine the properties of real fractal surfaces. In [8], the presence of a pronounced hysteresis of the normal force and contact angle in liquid bridges between two identical surfaces was experimentally shown when they approached and moved away in the normal direction at different speeds, from 0.02 to 2 mm/s. The review article [11] provides a brief description of the theoretical and experimental results on this topic. In [6, 10], various situations are considered in which a drop of liquid slides along an inclined plane, due to which different contact angles are observed at the leading and trailing fronts of motion. Similar situation is considered in the present work, with the difference that this is not a drop but a capillary bridge between two solids which is sliding.

In the present paper, following the preprint of one of the authors, [12], we present a simple theory describing the shape of the sliding capillary bridge and provide a detailed experimental study of the contact angle deformation due to contact angle hysteresis.

2. Basic Geometry of a Capillary Bridge

We consider a rigid sphere with radius R in contact with a solid surface with a small amount of a liquid in between (Fig.1).

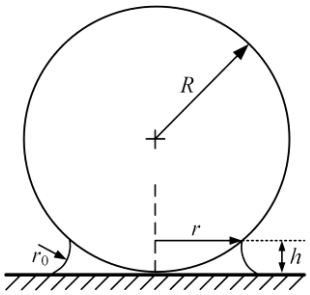

Fig. 1 A capillary bridge between a rigid plane and a rigid sphere

In equilibrium, the liquid forms a capillary bridge, which has two radii of curvature (Fig. 1). The larger radius r is always positive. The sign of the smaller radius r_0 depends on whether the contact angle is larger or smaller than $\pi/2$. For small contact angles, in the case of wetting of the surface, r_0 is negative. There is a reduced pressure in the liquid, which leads to a force that we call capillary force. In the most cases one can assume $|r_0| << r$, the differences between the pressure inside and outside the contact can be written as [4]

$$\Delta p = -\frac{\gamma}{r_0}, \tag{1}$$

where γ is the surface tension of the liquid. Note that in the equilibrium or at slow (quasistatic) sliding, the pressure in the liquid should be constant. This means, that the radius of curvature r_0 should be constant along the whole boundary line of liquid.

Fig. 2 Geometry of a capillary bridge

Fig. 2 displays the geometry of the contact angles and meniscus of a capillary bridge. It can be easily seen that the following geometrical relation is valid:

$$r_0(\cos\theta_1 + \cos\theta_2) = h. \tag{2}$$

The contact angles can be obtained from the equilibrium conditions for the boundary line, considering that each interface is acting on the boundary with a linear force density equal to the specific interface energy [4], see Fig. 3:

$$\gamma_{1,s} = \gamma_{1,l} + \gamma\cos\theta_1, \tag{3}$$

$$\gamma_{2,s} = \gamma_{2,l} + \gamma\cos\theta_2, \tag{4}$$

which gives for the contact angles

$$\cos\theta_1 = \frac{\gamma_{1,s} - \gamma_{1,l}}{\gamma}, \tag{5}$$

$$\cos\theta_2 = \frac{\gamma_{2,s} - \gamma_{2,l}}{\gamma}. \tag{6}$$

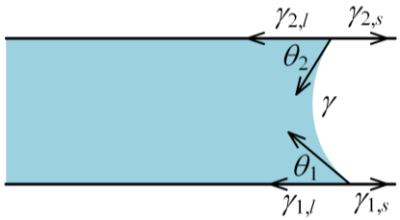

Fig. 3 Scheme of tension forces acting at the boundary of a liquid bridge. $\gamma_{1,l}$ and $\gamma_{1,s}$ are the surface energies of the first solid in contact with liquid and the atmosphere, correspondingly. Similar notations are valid for the second body. γ is the surface tension of liquid

Eqs. (5) and (6) are valid in thermodynamic equilibrium. If the boundary of the bridge is moving, it can experience a force of dry friction similar to that described for adhesive contacts in [13]. In the present paper, we will for simplicity assume that such dry friction force does act only on the boundary of a fluid in contact with body 1. That means that the second body is considered as being very smooth and chemically homogeneous, so that the contact angle hysteresis on its surface can be neglected. In the presence of friction force, Eq. (3) will take the form

$$\gamma_{1,s} = \gamma_{1,l} + \gamma\cos\theta_1 \pm f\ , \tag{7}$$

where f is the linear density of the force of friction. The sign "+" should be used if the right boundary of liquid is moving to the right and "–" if it is moving to the left. For the left boundary, the use of sign is inverse to the above stated. From Eq. (7), it follows

$$\cos\theta_1 = \frac{\gamma_{1,s} - \gamma_{1,l} \mp f}{\gamma}\ . \tag{8}$$

Substituting Eqs. (1), (6) and (8) into Eq. (2) gives

$$h = \frac{\gamma_{1,s} + \gamma_{2,s} - \gamma_{1,l} - \gamma_{2,l} \mp f}{|\Delta p|} = \frac{\gamma^* \mp f}{|\Delta p|} \tag{9}$$

with $\gamma^* = \gamma_{1,s} + \gamma_{2,s} - \gamma_{1,l} - \gamma_{2,l}$.

Note that Eq. (7) and the following Eq. (9) do not depend on whether the contact angle is larger or smaller $\pi/2$.

3. Shape of the Contact Area for Friction Perpendicular to the Boundary Line

The force of friction acting on the boundary line may depend on the nature of this force. Two limiting cases can be considered. If the microscopic heterogeneity is moderate, then the movement of the liquid in the direction of the boundary line will occur without instabilities. However, the appearance of instabilities is a necessary precondition for appearance of static force of friction [13]. This means, that the movement along the boundary does not lead to friction. The movement in the direction perpendicular to the boundary, on the contrary, will always lead to appearance of instable configurations followed by rapid jumps and energy dissipation. On the macroscopic scale, this energy dissipation is perceived as being due to static force of friction. Under the conditions described, the force of friction is always directed perpendicularly to the boundary, as shown in Fig. 4. Moreover, the magnitude of the force of friction does not depend on the velocity, so that the force line density is constant in all boundary points. However, its direction changes abruptly at the side points of the contact where the direction of movement is parallel to the boundary line.

From Eq. (9), it follows that the height of the gap on the front side of contact is constant and equal to

$$h_{\text{front}} = \frac{\gamma^* - f}{|\Delta p|}\ , \tag{10}$$

while at the back side it is

$$h_{\text{back}} = \frac{\gamma^* + f}{|\Delta p|} . \tag{11}$$

In the following, we consider a contact between a parabolic body $z(r) = r^2/(2R)$, where z is the normal coordinate and r polar radius in the contact plane. For such body, Eqs (10) and (11) mean that the contact area has constant (but different) radii on the front and back side of the contact, Fig. 4b:

$$a_{0,\text{front}} = \sqrt{2R\frac{\gamma^* - f}{|\Delta p|}} , \quad a_{0,\text{back}} = \sqrt{2R\frac{\gamma^* + f}{|\Delta p|}} . \tag{12}$$

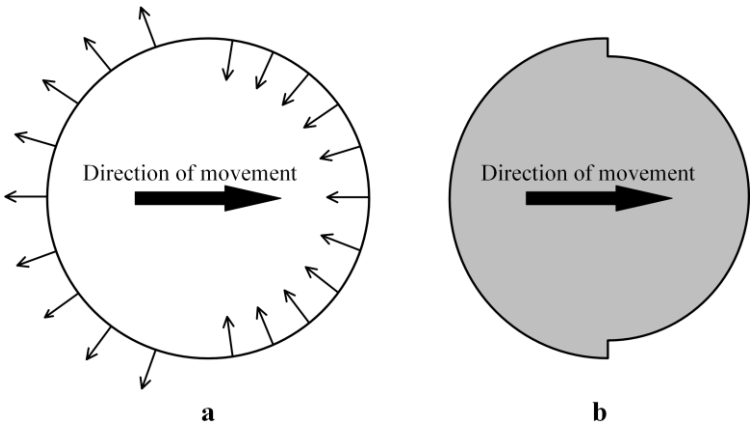

Fig. 4 (a) Friction forces acting on the boundary of liquid when the capillary contact is moving to the right; (b) Shape of the contact area in the case of constant friction force directed perpendicular to the boundary of liquid

Note that the pressure difference Δp can change during the movement to maintain the given volume of interfacial liquid. However, the change of volume at a constant Δp is zero in the linear approximation, so that if the force of friction is small, then the pressure difference can be considered as unchanged. In the same approximation, the total force of friction can be evaluated as

$$F_{\text{Friction}} = 2\int_0^{\pi/2} (a_{0,\text{front}} + a_{0,\text{back}})\, f \cos\varphi \mathrm{d}\varphi = 2(a_{0,\text{front}} + a_{0,\text{back}})\, f . \tag{13}$$

Definition of the angle φ is given in Fig. 5. For small friction force,

$$\frac{a_{0,\text{front}} + a_{0,\text{back}}}{2} \approx a_0 = \sqrt{2R\frac{\gamma^*}{|\Delta p|}} \tag{14}$$

and the total friction force can be obtained in the first order by integrating the force density over the unperturbed shape of the contact (circle):

$$F_{\text{Friction}} = 4a_0 f . \tag{15}$$

4. Shape of the Contact Area for Friction Opposite to the Direction of Motion

Principally thinkable is also another law of friction for the boundary line. If the microscopic heterogeneity of the substrate becomes large, this will lead to comparable changes in the configuration of the boundary line, independently on the direction of its movement. This means, that the force of friction will be directed oppositely to the direction of motion, as shown in Fig. 5a. However, for the contact angle, only the component of the friction force perpendicular to the boundary line is relevant. This component is equal to

$$f_{\perp} = f\cos\varphi\,. \tag{16}$$

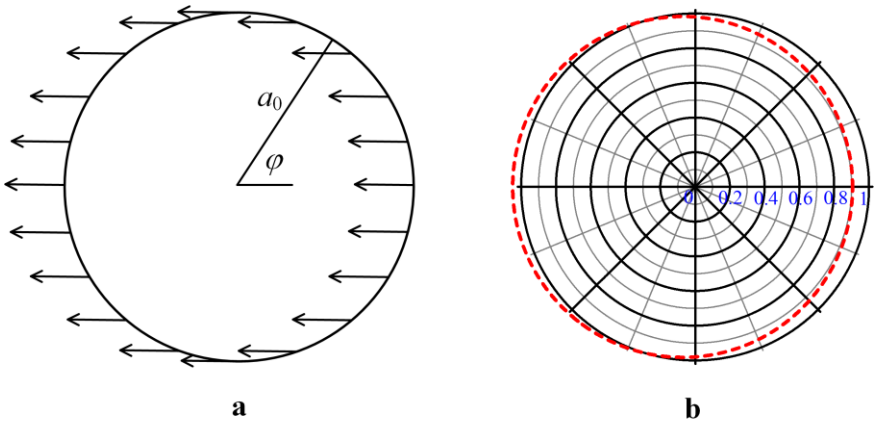

Fig. 5 Case of friction opposite to the direction of motion: (a) Forces acting on the boundary line, (b) shape of the contact area (dashed line)

Eqs. (12) change to

$$a_0(\varphi) = \sqrt{2R\frac{\gamma^* - f\cos\varphi}{|\Delta p|}}\,. \tag{17}$$

This dependency is shown in Fig. 5b. While the shape of the contact is asymmetrical also in this case, the asymmetry is barely visible and manifests itself mostly in the shifting the contact area from the center of the body in the direction opposite to the direction of sliding. The force of friction can be estimated as $F_{\text{Friction}} = 2\pi a_0 f$, provided that the deviation of the shape of the boundary from the circle is not too large.

5. Experiment

Experiments have been conducted using the setup depicted in Fig. 6. Steel spheres having various radii of curvature were moved vertically and tangentially with precision linear stages M-403.2DG. For recording normal and tangential forces, a strain gage sensor ME K3D40 was mounted between the sample and the moving stages. The contact region was illuminated from the side with 80 LEDs and was recorded from underneath

using a digital camera with resolution of 1600 x 1200 pixels. An inclination mechanism was used to ensure parallel orientation between the glass surface and tangential indenter movement.

In each experiment, the following operations have been performed. First, a drop of liquid was placed on a smooth sheet of a silicate glass. Then, an indenter of radius R approached the glass plate in the normal direction with a small velocity of v = 10 μm/s. The indenter was moved towards the glass as close as possible, but direct contact between the indenter and the glass was avoided. After finishing the approaching phase, indenter was moved in the tangential direction with velocity 10 μm/s by a distance of x = 10 mm. Subsequently, it was moved in the opposite direction to the initial position x = 0 mm. Cow's milk with 3.5% fat was used as liquid. It was chosen because milk is not transparent, which made it possible to accurately observe the evolution of contact boundary and contact form during sliding. As indenters two spherical bodies with radii R = 100 mm and R = 33 mm have been used. Since the indenter was not in direct contact with the substrate, the normal force F_N was negative due to capillary effects. It was approximately –15 mN for indenter with R = 33 mm and –40 mN for the indenter with radius R = 100 mm.

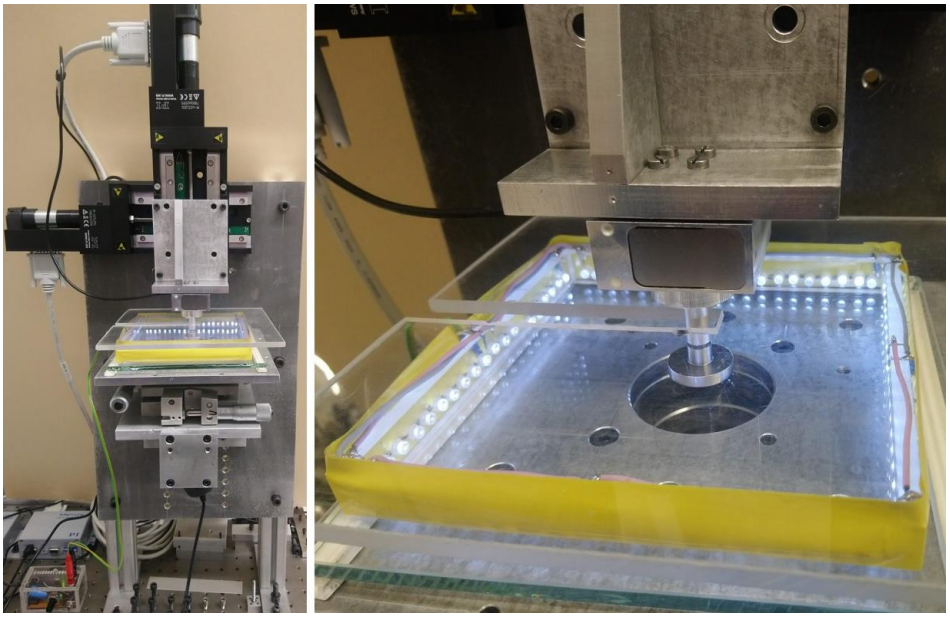

Fig. 6 Experimental set-up for observing contact configuration of a capillary bridge [14, 15]. Left panel – general view, right panel – contact between steel indenter and substrate, with lighting system

A series of 5 experiments was performed for each indenter. In the first experiment, a smooth glass was used. In three subsequent experiments, the glass had been roughened by machining with sandpaper having numbers P180, P80 and P40. These numbers, according to the standard classification, correspond to the average sandpaper grain size of 82, 201

and 425 μm, respectively. The last (fifth) experiment was carried out after an even more intensive processing of the glass surface with P40 paper, which further increased the roughness value. The results obtained in the last fifth experiment will be denoted as "P40+".

Results for indenter with radius of curvature R = 33 mm

In this series, a stainless-steel spherical indenter with a radius of R = 33 mm was used. The surface of the indenter was polished to a mirror finish. Fig. 7 shows the dependence of the experimentally measured normal and tangential contact forces on time in all five experiments of a series. In both panels of the figure, three vertical dashed lines are introduced, delimiting various stages of the experiment. Before the first dashed line, the indenter approaches the glass substrate in the normal direction. Displacement in the tangential direction takes place between the first and the second lines. After the second vertical line, the indenter starts moving in the opposite direction. The third line marks the moment of time when the indenter stops moving horizontally and is lifted to the initial position.

From Fig. 7b, it follows that the tangential force F_x remains almost zero over the entire time range. In any case, it is smaller than the random background noise of the force sensor used. The normal force F_N, on the contrary, can be clearly resolved and takes negative values due to capillary effects. In the experiment, the glass substrate is not perfectly flat, and the indenter cannot be shifted ideally parallel to the substrate surface. Therefore, changes in the force F_N during tangential motion up to the second vertical line (before changing the direction of movement of the indenter) can be associated with a change in the distance between the indenter and the glass. However, a more detailed analysis of the dependences in Fig. 7a shows that the magnitude of the normal force, $|F_N|$, is smaller after changing the direction of movement. This effect cannot be explained by the changing distance between the glass plate and the indenter since the reverse movement of the indenter in the tangential direction occurs along the same trajectory as its forward movement. To find out the reasons for this behavior, it is necessary to analyze the behavior of the observed contact area.

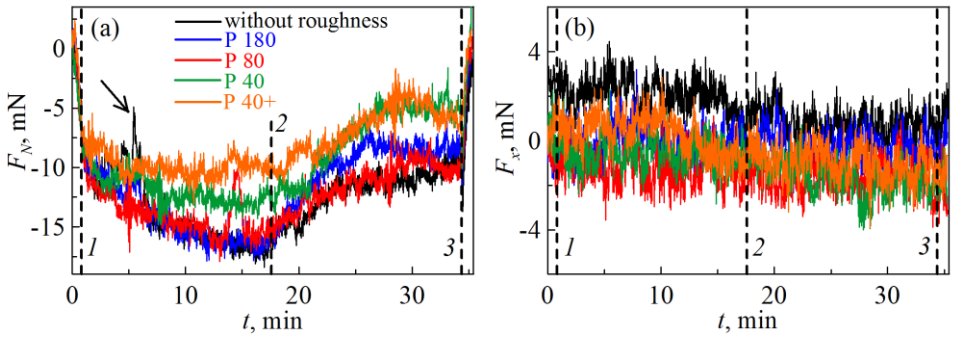

Fig. 7 Dependences of the normal F_N (a) and tangential F_x (b) forces acting on the indenter in the experiment with an indenter with a radius of R = 33 mm on time t

The contact area versus time for the case of a smooth glass substrate is shown in Fig. 8, left panel. The figure shows both the full area and the area to the right and to the left from the center line of indenter (visualized by a vertical dashed line in Fig. 8, right panel). The right panel of Fig. 8 shows the snapshots of the contact shape at the time moments marked with letters in the left panel. It is clearly seen that the area of the sliding contact is divided into regions with smaller radius (front part of the contact area) and a larger radius (back part) with a rapid transition between both parts. This strongly resembles the predicted shape shown in Fig. 4. This means, that the correct assumption is that friction force is directed perpendicular to the border line and has a jump at the "turning point". However, experiment shows details which are not predicted, and which have to be mentioned and discussed.

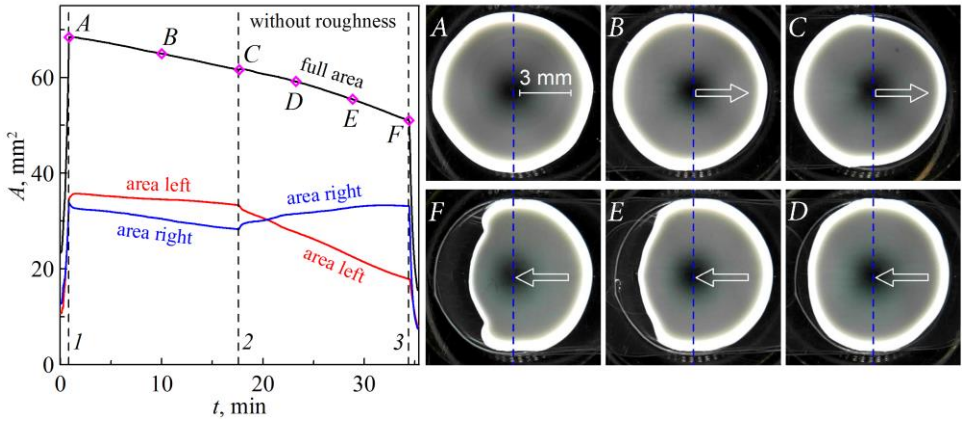

Fig. 8 Left panel: time dependencies of the full area of the contact, as well as the area to the left and to the right from the center line of the indenter. Right panel: photographs of the contact area corresponding to the time moments marked with letters in the left panel

First, note that the total area of the contact decreases with time. This is due to the fact that some portion of the liquid remains behind the actual capillary bridge. These rests are visible by the changed color of the glass. Further, attentive consideration of videos [16, 17] shows that the changes in shape of the front part of the bridge occur not at once. For some time, the bridge keeps the circle shape before it starts to reshape. At the border of the initial contact area, a distinct track remains, suggesting that we have here with a sort of pinning. It looks that we have to do with a static (pinning) force which is higher than the subsequent boundary force during sliding. Further, there exist a distinct difference between the shape of the capillary bridge during the initial sliding and the "back sliding". In initial sliding, the movement of the front boundary (Fig. 8, right upper panel) occurs much jerkier, but at the same time, the deviation from the circle shape is smaller than by the back movement. Quite obviously, this is related to the fact, that the surface properties change after the first passing of the drop. Interestingly, the jerky movement is not correlated with the boundary friction force, judging by the asymmetry of the contact shape. Thus, the friction force is in this case caused not by the macroscopic roughness or heterogeneity but is determined by a lower, microscopic, scale. This is confirmed by the

fact, that the roughness changes substantially the well visible mesoscopic heterogeneity of the movement of the border line (which is in the case of rougher surfaces much jerkier) but practically does not influence the overall appearance of the contact shape.

Video [16] shows in detail the movement of the contact region in all 5 experiments with different roughness of the glass substrate for an indenter with radius R = 33 mm. Video [17] contains similar data for an indenter with radius R = 100 mm. Comparison of results of all experiments allows to conclude that the roughness and the indenter radius do not qualitatively change the behavior described above (Fig. 8). The main effect of the increasing roughness is that the propagation of the contact becomes more discontinuous. The main effect of the radius of curvature is that in the case of a larger radius R = 100 mm, at the initial approach of the indenter to the glass, a drop of liquid often spreads nonuniformly. However, after some transient regime the stationary sliding resembles the situation shown in Fig. 8. A detailed analysis of all details of the kinetics and properties of the stationary sliding will be published elsewhere, but the data of all experiments are already available in [16, 17].

6. CONCLUSIONS

We considered the changes in the shape of the contact area of a capillary bridge when it is sliding in tangential direction. Due to the friction force acting in the boundary, the contact area becomes asymmetric. Two limiting laws of friction have been considered: (a) with force of friction acting perpendicular to the boundary line and (b) opposite to the direction of sliding. The predicted shapes are substantially different. This means that experimental study of the shape of capillary bridges can give information about the character of the friction law in the boundary line. Experimental investigation confirms a jump-like shape for smoother indenters and more continuous for rougher indenters which mean that there may be a transition between the laws of friction (a) and (b) with increasing roughness. In the present paper, we assumed that one solid surface exhibits no friction with the liquid. This assumption can be dropped as in the general case all theoretical results remain the same with $f = f_1 + f_2$.

Acknowledgement: *This research was partially supported by "The Tomsk State University competitiveness improvement program" and by Deutsche Forschungsgemeinschaft (Project DFG PO 810-55-1). We thank one of the reviewers who made us aware that the assumption that one of the solid surfaces exhibits no friction can be dropped.*

REFERENCES

1. Bowden, F. P., Tabor, D., 2001, *The Friction and Lubrication of Solids*, Clarendon Press.
2. Popova, E., Popov, V.L., 2015, *The research works of Coulomb and Amontons and generalized laws of friction*, Friction, 3(2), pp. 183-190.
3. Persson, B.N.J., 2002, Sliding Friction. Physical Principles and Applications, Springer.
4. Popov, V.L., 2017, *Contact Mechanics and Friction. Physical Principles and Applications, 2nd Edition*, Berlin: Springer.
5. Semprebon, C., McHaleb, G., Kusumaatmaja, H., 2017, *Apparent contact angle and contact angle hysteresis on liquid infused surfaces*, Soft Matter, 13(1), pp. 101-110.
6. Gao, L., McCarthy, T.J., 2006, *Contact angle hysteresis explained*, Langmuir, 22, pp. 6234-6237.

7. Junchao, W., Wu, Y., Cao, Y., Li, G., Liao, Y., 2020, *Influence of surface roughness on contact angle hysteresis and spreading work*, Colloid and Polymer Science, 298, pp. 1107-1112.
8. Shia, Z., Zhang, Y., Liu, M., Hanaor, D.A.H., Gan, Y., 2018, *Dynamic contact angle hysteresis in liquid bridges*, Colloids and Surfaces A: Physicochemical and Engineering Aspects, 555, pp. 365-371.
9. Heib, F., Schmitt, M., 2016, *Statistical contact angle analyses with the high-precision drop shape analysis (HPDSA) approach: basic principles and applications*, Coatings, 6(4), 57.
10. Wu, C.-J., Li, Y.-F., Woon, W.-Y., Sheng, Y.-J., Tsao, H.-K., 2016, *Contact angle hysteresis on graphene surfaces and hysteresis-free behavior on oil-infused graphite surfaces*, Applied Surface Science, 385, pp. 153-161.
11. Hubbe, M.A., Gardner, D.J., Shen, W., 2015, *Contact angles and wettability of cellulosic surfaces: A review of proposed mechanisms and test strategies*, BioResources, 10(4), pp. 8657-8749.
12. Popov, V.L., 2020, *Shape of a sliding capillary contact*, arXiv:2012.13979, http://arxiv.org/abs/2012.13979
13. *Popov, V.L.*, Adhesion hysteresis due to chemical heterogeneity. In: Multiscale Biomechanics and Tribology of Inorganic and Organic Systems, Eds. Ostermeyer, Popov, Shilko, Vasiljeva, Springer, 2021, pp. 473-483.
14. Lyashenko, I.A., Pohrt, R., 2020, *Adhesion between rigid indenter and soft rubber layer: Influence of roughness*, Frontiers in Mechanical Engineering. Section Tribology, 6, 49.
15. Lyashenko, I.A., Popov, V.L., 2020, *The effect of contact duration and indentation depth on adhesion strength: experiment and numerical simulation*, Technical Physics, 65(10), pp. 1695-1707.
16. Popov, V.L., Lyashenko, I.A., Starcevic, J., 2021, *Shape of a sliding capillary contact due to hysteresis of contact angle (experiment with indenter R=33mm)*, supplementary video. https://doi.org/10.13140/RG.2.2.13032.49923
17. Popov, V.L., Lyashenko, I.A., Starcevic, J., 2021, *Shape of a sliding capillary contact due to hysteresis of contact angle (experiment with indenter R=100mm)*, supplementary video. https://doi.org/10.13140/RG.2.2.33165.15840